The Meteoritical Society

*Meteoritics & Planetary Science* 45, Nr 4, 596–614 (2010)
doi: 10.1111/j.1945-5100.2010.01045.x

# Structural and isotopic microanalysis of presolar SiC from supernovae

K. Mairin HYNES*, T. Kevin CROAT, Sachiko AMARI, Aaron F. MERTZ[1], and Thomas J. BERNATOWICZ

Laboratory for Space Sciences and the Physics Department, Washington University, One Brookings Drive, St. Louis, Missouri 63130, USA
[1]Present address: Department of Physics, Yale University, PO Box 208120, New Haven, Connecticut 06520, USA.
*Corresponding author. E-mail: kmhynes@wustl.edu

(*Received 29 June 2009; revision accepted 08 February 2010*)

**Abstract**–We report on the microstructure, crystallography, chemistry, and isotopic compositions of seven SiC X grains and two mainstream grains from the Murchison meteorite. TEM crystallographic analysis revealed that the X grains (approximately 3 μm) are composed of many small crystals (24–457 nm), while the similarly sized mainstream grains are composed of only a few crystals (0.5–1.7 μm). The difference in crystal size likely results from differences in their formation environments: the X grain crystals evidently formed under conditions of greater supersaturation and rapid growth compared to their mainstream counterparts. However, the same polytypes are observed in both mainstream and X grains. Six X grains and both mainstream grains are entirely the 3C-SiC polytype and one X grain is an intergrowth of the 3C-SiC and 2H-SiC polytypes. EDXS measurements indicate relatively high Mg content in the X grains ($\lesssim$5 atomic%), while Mg was undetectable in the mainstream grains. The high Mg content is probably from the decay of $^{26}$Al into $^{26}$Mg. Estimates of the $^{26}$Al/$^{27}$Al ratios, which range from 0.44–0.67, were made from elemental Mg/Al ratios. This range is consistent with the $^{26}$Al/$^{27}$Al ratios inferred from previous isotopic measurements of X grains. We also report the first direct observations of subgrains in X grains, including the first silicides [$(Fe,Ni)_nSi_m$]. Diffraction data do not match any previously observed presolar phases, but are a good fit to silicides, which are predicted stable SN condensates. Eight subgrains with highly variable Ni/Fe ratios (0.12–1.60) were observed in two X grains.

## INTRODUCTION

Isotopic studies of presolar grains provide important information about stellar nucleosynthesis at an unprecedented level of detail (see Meyer and Zinner 2006). In addition, chemical, structural, and mineralogical microanalysis can offer valuable insights into grain formation in circumstellar outflows and supernovae (SNe) ejecta (see Bernatowicz et al. 2006). Laboratory studies indicate that the microstructural characteristics of presolar SiC grains are dependent upon the physical conditions, such as temperature and pressure, in which they condense. Detailed morphological studies on presolar SiC therefore provide important information for understanding the conditions in which these grains form at a level of detail that cannot be obtained through astronomical observation alone (Daulton et al. 2003; Croat et al. 2005).

For the most complete constraints on presolar grain formation, detailed structural and chemical microanalytical studies can be combined with isotopic measurements. An example of this analytical approach is the study by Croat et al. (2003) of ultramicrotome sections of SN graphite grains from the Murchison meteorite. Isotopic characterization with nano-scale secondary ion mass spectrometry (NanoSIMS) revealed large excesses in $^{18}$O and $^{28}$Si, indicating a SN origin. Microanalysis of the same presolar graphite sections with a transmission electron microscope (TEM) revealed the presence of internal TiC subgrains, which NanoSIMS analysis subsequently confirmed to be of presolar origin based on large Ti isotopic anomalies.

These internal subgrains were found in all of the SN graphite grains studied, with a single graphite grain containing up to several hundred TiC subgrains. Some of these internal TiC subgrains have attached iron-nickel grains epitaxially grown onto one or more of the TiC faces. Further analysis of the chemistry, morphology, and crystallography of the SN graphite grains and their internal subgrains allowed inferences to be drawn concerning the physical conditions of the gas from which these graphite grains condensed. For example, grain morphology indicates the condensation sequence, with TiC condensing first, followed by the iron-nickel phases, and finally graphite. This sequence places bounds on the temperature and pressure of the gas in which these grains condensed. Additionally, the properties of the TiC subgrains were used to determine the minimum Ti number densities in the gas before condensation and suggest that turbulent mixing must have occurred in the SN outflows prior to TiC incorporation in the graphite.

In addition to the information learned from studying SN graphite grains, further understanding of SN outflows can be gained by studying another type of presolar grain with a SN origin, SiC X grains (Amari et al. 1992). While $\geq$95% of presolar SiC grains originate in the outflows of asymptotic giant branch (AGB) stars, X grains comprise only approximately 1% of all presolar SiC grains. The primary indicator of a SN origin for SiC X grains is large excesses of $^{28}$Si, which can only be produced deep within the interiors of massive stars (see Meyer and Zinner 2006). Most X grains are also characterized by isotopically light C ($^{12}$C/$^{13}$C > Solar = 89) and isotopically heavy N ($^{14}$N/$^{15}$N < Solar = 272), both of which are the result of nucleosynthesis in massive stars. These isotopic compositions are distinct from those of grains originating around AGB stars, so-called mainstream grains, which constitute most of the presolar SiC population ($^{29}$Si/$^{28}$Si, $^{30}$Si/$^{28}$Si, $^{14}$N/$^{15}$N > Solar; 10 < $^{12}$C/$^{13}$C < 100) (see Meyer and Zinner 2006). Some X grains also contain radiogenic isotopes from nuclides that are only produced in SNe, such as $^{44}$Ca from the decay of $^{44}$Ti (Nittler et al. 1996) and $^{49}$Ti from the decay of $^{49}$V (Hoppe and Besmehn 2002).

Unlike presolar graphite, which has only one basic crystal structure that occurs in varying degrees of structural perfection, SiC has approximately 250 crystal structures, or polytypes, which depend on the particular repetitive stacking sequence of Si-C bilayers (Kern et al. 1998). Most of these polytypes have only been produced in laboratories and only a few have ever been observed in nature. SiC polytypes are sometimes grouped into two categories: the unique cubic 3C polytype (also called β-SiC) and the hexagonal and rhombohedral polytypes (all the others collectively called α-SiC). For a thorough discussion of SiC polytypes, see Daulton et al. (2003).

Because the formation of particular presolar SiC polytypes is determined by the physical conditions of the stellar outflows in which the grains condense, knowledge of the microstructure of presolar SiC can provide valuable insight into formation conditions. Astronomical data is of limited use in this regard, however. Infrared spectra can, at most, distinguish between the α-SiC and β-SiC polytypes and even the ability to make this distinction is subject to controversy (Speck et al. 1999). However, SiC polytypes can be distinguished from one another in the TEM. Utilizing analytical and high-resolution TEM to determine the polytypes of 508 randomly selected Murchison presolar SiC grains (500 nm average size), Daulton et al. (2003) observed only two polytypes: the cubic 3C (fcc; $a$ = 4.36 Å) polytype (approximately 79% by number) and the hexagonal 2H ($a$ = 3.08 Å, $c$ = 5.03 Å) polytype (approximately 3%), as well as intergrowths of these two polytypes (approximately 17%). Most of these SiC grains are single crystals, while the rest are twinned. A small number (approximately 1%) of one-dimensionally disordered SiC grains could not be classified as any polytype. Because >90% of Murchison SiC grains are mainstream grains and because coordinated isotopic data have been obtained for only a small number of these SiC grains (Daulton et al. 2006, 2009), to first order, this polytype distribution largely represents mainstream SiC grains, which formed around AGB stars.

Laboratory studies of SiC growth show that the 2H polytype has the smallest unit cell and generally the lowest formation temperature, followed by 3C, and then by the higher-order rhombohedral and hexagonal polytypes. The temperatures at which the 2H and 3C polytypes form and remain stable in laboratory experiments are roughly consistent with theoretical equilibrium thermodynamics predictions for the circumstellar outflows of AGB stars (Lodders and Fegley 1995; Sharp and Wasserburg 1995). However, the higher number densities in SN outflows could conceivably result in the formation of higher-order polytypes in some SiC X grains, which may not have been observed by Daulton et al. due to the small number of X grains encountered in their study (presumably approximately 1% of the total).

While the polytype distribution of mainstream grains is well understood, very little is known about the microstructure of the minor types of presolar SiC, including X grains. Only one morphological study has previously been done on SiC X grains. Utilizing a focused ion beam lift-out, Stroud et al. (2004) analyzed

two X grains with the TEM. One grain is the 3C polytype, while the other is the 2H polytype. No higher-order polytypes were observed. Although several previous presolar SiC microanalytical studies (Bernatowicz et al. 1992; Stroud et al. 2002; Stroud and Bernatowicz 2005; R. Stroud, personal communication) have observed internal (Ti,V)C, AlN, Fe, Fe-Ni, and graphite subgrains in presolar SiC, all of these grains (three mainstream grains and one Z grain) originated in the outflows of AGB stars. In the Stroud et al. (2004) X grain study, no subgrains were found.

In this study, we present a coordinated TEM and NanoSIMS study of seven SiC X grains from the Murchison CM2 meteorite. These grains were selected on the basis of their isotopic compositions, namely large $^{28}$Si excesses, which were determined by NanoSIMS analysis. The seven X grains were then analyzed in the TEM for their chemical composition and structural characteristics, including polytype, crystal domain size, and subgrains. Two mainstream grains from the same size fraction as the X grains were also selected for TEM analysis to provide a basis for comparison with the X grains. The combined microstructural, isotopic, mineralogical, and chemical data on these X grains yield insights into the formation of SiC grains in SN outflows.

## EXPERIMENTAL METHODS

### Isotopic Characterization

Silicon carbide grains were obtained from the KJG size separate (2.1–4.5 μm observed size) of the Murchison meteorite (Amari et al. 1994). An aggregate of grains was dropped onto a Au foil and subsequently analyzed for Si isotopes in a Cameca IMS 3f ion microprobe utilizing ion imaging to locate potential X grains (Amari et al. 2000). Because the IMS 3f has relatively low sensitivity, grains that had $^{28}$Si/$^{30}$Si ratios greater than the solar value (29.75) were subsequently analyzed in a Cameca NanoSIMS with high mass resolution and high sensitivity to verify their grain type. Negative secondary ions of C, Si, and in some cases CN (for the N isotopes) were measured with a $Cs^+$ beam. No additional isotopes were measured with the NanoSIMS in order to minimize grain sputtering and to preserve as much of the grain as possible for subsequent analysis in the TEM. Mainstream SiC grains, also from the KJG size fraction of the Murchison meteorite, were similarly analyzed in the NanoSIMS for their C, Si, and N isotopic compositions.

### TEM Sample Preparation and Characterization

After isotopic characterization, the grains were imaged in a JEOL 840A SEM to locate their positions on the grain mount. Seven SiC X grains and two mainstream grains were subsequently selected for study in the TEM. Each of the selected grains was picked from the ion probe mount with a sharpened tungsten needle held in a micromanipulator. The tip of the needle was kept clean and at a diameter of approximately 1 μm by electrochemically sharpening the needle with a solution of sodium hydroxide. Utilizing an optical microscope to view the process, we placed each SiC grain at the bottom of a gelatin capsule, along with three carbon fibers to later aid in locating the grain. The capsule was slowly filled with LR White Hard resin and cured at 60 °C for 24 h. The gelatin capsule was then removed, leaving the SiC grain and the carbon markers embedded in the resin block. The top of the resin block was trimmed into a multi-step pyramid with a Reichert-Jung Ultracut E microtome equipped with a glass knife, with the top step having a side-length of approximately 0.5 mm and containing the SiC grain and the carbon markers. The top step was then sliced with the ultramicrotome fitted with a diamond knife attached to a water reservoir. The 70 nm thick slices of SiC and the surrounding resin were removed from the water's surface with Pella 3 mm, 75 mesh Cu TEM grids covered with Formvar stabilized with carbon.

The microstructure and chemical composition of the SiC and their internal grains were determined with a JEOL 2000FX TEM equipped with a NORAN Vantage energy-dispersive X-ray spectrometer (EDXS). The Novar window of the EDXS allowed identification of all elements with $Z \geq 5$. Background and peak fitting were performed on these spectra with Origin-based in-house software, described by Croat et al. (2003). In cases where elemental peaks (such as Al or Mg) were not detected, an upper limit of $2\sigma$ of the background counts in the energy region of interest was placed on their concentrations. Quantitative analyses were performed with k-factors for Al, Si, and Mg determined from a geologic standard (basaltic glass USNM 113498).

The polytype was determined for each SiC grain utilizing both selected-area diffraction (SAD) and convergent-beam electron-diffraction (CBED) patterns. Low-index zones were located by tilting the crystals along both orthogonal axes of the sample stage goniometer. The diffraction patterns were subsequently analyzed to determine the polytype of each crystal.

Since inclusions of other phases contained within the SiC X grains were of interest, each slice was observed at high magnification (approximately $10^5\times$) while the crystal was systematically rotated through $\pm 30°$ about one axis

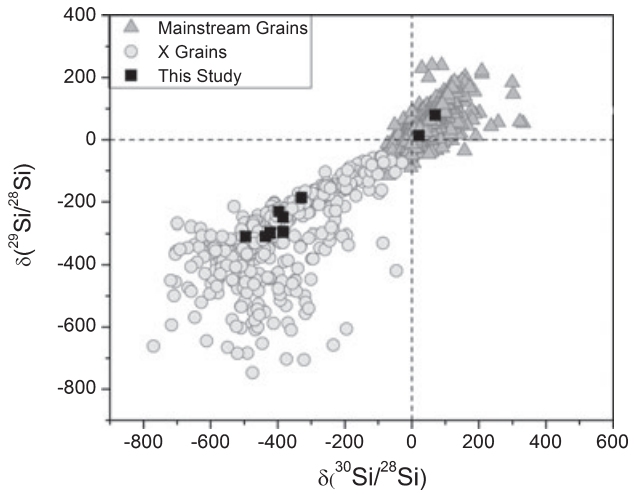


Fig. 1. Plot of the Si isotopic ratios of the seven X grains and two mainstream grains in this study expressed as δ-values, or deviations from the solar isotopic ratio in parts per thousand (‰). The grains are plotted against isotopic data from other X grains and mainstream grains for comparison (grain data is from the Presolar Database [Hynes and Gyngard 2009]).

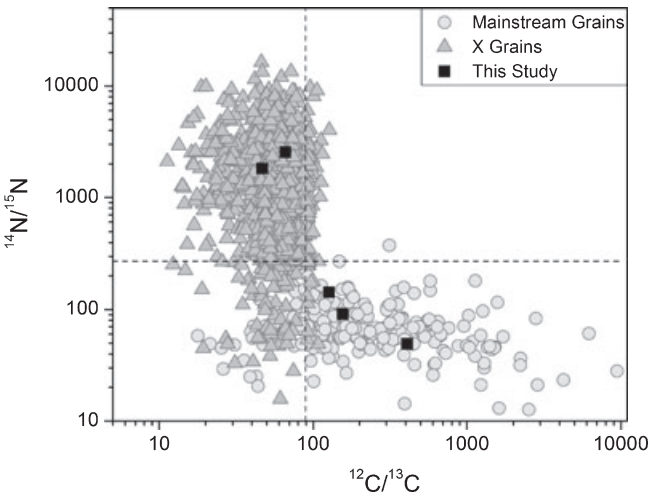


Fig. 2. Plot of the C and N isotopic ratios of three X grains and both mainstream grains from this study; N isotopic data are not available for the other grains. As in Fig. 1, the grains are plotted against isotopic data from other X grains and mainstream grains for comparison.

Table 1. Isotopic compositions of X grains and mainstream grains in this study (±1 σ errors).

| Grain label | Type | $^{12}C/^{13}C$ | $^{14}N/^{15}N$ | $\delta^{29}Si/^{28}Si$[a] (‰) | $\delta^{30}Si/^{28}Si$[a] (‰) |
|---|---|---|---|---|---|
| KJG-N2-31-1 | X | 250 ± 4 | | −309 ± 4 | −436 ± 5 |
| KJG-N2-129-1 | X | 111 ± 1 | | −187 ± 5 | −329 ± 6 |
| KJG-N2-253-2 | X | 162 ± 2 | | −231 ± 5 | −396 ± 6 |
| KJG-N2-411-2 | X | 216 ± 3 | | −298 ± 5 | −422 ± 6 |
| KJG-N4-185-1 | X | 127 ± 0.5 | 144 ± 1 | −296 ± 3 | −384 ± 4 |
| KJG-N4-263-1 | X | 156 ± 0.6 | 91 ± 1 | −249 ± 2 | −384 ± 3 |
| KJG-N4-585-2 | X | 409 ± 2 | 49 ± 0.5 | −310 ± 3 | −495 ± 4 |
| KJG-N4-439-2 | Mainstream | 47 ± 0.2 | 1818 ± 72 | 79 ± 3 | 70 ± 4 |
| KJG-N4-595-1 | Mainstream | 66 ± 0.2 | 2535 ± 80 | 12 ± 3 | 22 ± 4 |

Notes: [a]Values given in "delta" notation, defined as: $\delta^{i}X/^{j}X \equiv [(^{i}X/^{j}X)_{measured}/(^{i}X/^{j}X)_{\odot} - 1] \times 1000$.

of the sample stage goniometer. Diffraction contrast was used to identify candidate internal grains and their compositions were subsequently determined with EDXS. Once located, the grains were rotated to low index crystallographic zones from which CBED patterns were obtained. The known d-spacings of the surrounding SiC were used as a calibration standard for the d-spacings of internal grains. Utilizing this as the primary method of detection, internal grains as small as approximately 15 nm could be identified.

## RESULTS

### Isotopic Composition

Isotopic measurements on all X grains and mainstream grains, made prior to TEM analysis, are reported in Table 1. The large excesses in $^{28}Si$ relative to normal solar system ratios clearly identify seven of the grains as X grains. In addition, they are all more depleted in $^{30}Si$ than in $^{29}Si$ and lie near the line of slope 0.6 defined by most X grains on a $\delta^{29}Si/^{28}Si$ versus $\delta^{30}Si/^{28}Si$ three isotope plot (Fig. 1).

delta notation: $\delta^{i}X/^{j}X \equiv$

$$[(^{i}X/^{j}X)_{measured}/(^{i}X/^{j}X)_{\odot} - 1] \times 1000 \quad (1)$$

These are the type X1 grains defined by Lin et al. (2002), as opposed to X2 grains which have relatively larger $^{29}Si$ depletions. Most X grains plot well above the mixing line of slope 1 between solar system Si ($\delta^{i}Si/^{28}Si \equiv 0$) and pure $^{28}Si$ ($\delta^{i}Si/^{28}Si \equiv -1000$) (Nittler et al. 1995). The seven X grains from this study are enriched in $^{12}C$ and the three that were measured for their N isotopic compositions also showed $^{15}N$ enrichments (Fig. 2), typical of SiC X grains (Amari et al. 1992).

Table 2. EDXS measurements of Al and Mg elemental content of SiC X and mainstream grains.

| Grain label | Type | Atomic% Al | Atomic% Mg | Mg/Al |
|---|---|---|---|---|
| KJG-N2-31-1 | X | < 0.7 | < 0.2 | |
| KJG-N2-129-1 | X | 3.4 | 2.1 | 0.63 ± 0.05 |
| KJG-N2-253-2 | X | 1.4 | 0.6 | 0.43 ± 0.11 |
| KJG-N2-411-2 | X | 2.8 | 2.0 | 0.71 ± 0.08 |
| KJG-N4-185-1 | X | 6.5 | 5.0 | 0.74 ± 0.04 |
| KJG-N4-263-1 | X | 1.3 | < 0.15 | < 0.12 |
| KJG-N4-585-2 | X | 2.0 | 1.3 | 0.66 ± 0.05 |
| KJG-N4-439-2 | Mainstream | 1.7 | < 0.08 | < 0.05 |
| KJG-N4-595-1 | Mainstream | 1.5 | < 0.18 | < 0.12 |

Notes: Atomic% for Al and Mg are quantified for a grain assumed to be composed of only of Si, Al, and Mg. Carbon values are not quantified or included due to large background interferences from the grid substrate. Grain KJG-N2-31-1 is an intergrowth between the 3C-SiC and 2H-SiC polytypes; all other grains are the 3C-SiC polytype.

The two mainstream grains show enrichments in $^{13}C$, $^{14}N$, and $^{29,30}Si$ relative to the solar values, which are all indications of an AGB origin (Hoppe et al. 1994). Both the X grains and the mainstream grains in this study were selected as typical isotopic representatives of their respective grain types in order to make inferences about these grain populations, albeit from a limited sample size.

## Chemical Composition

After isotopic analysis in the NanoSIMS and ultramicrotomy, sections of each grain were analyzed in the TEM. An EDXS spectrum was acquired at several spots on each grain and for the grain as a whole. As expected, the spectra revealed mainly Si and C. Due to the large C background signal from the Formvar substrate and embedding resin, C is excluded from all elemental quantifications that follow.

Most of the SiC X grains (5 of 7) also contain minor amounts of both Al and Mg, ranging from 1.3–6.5 and 0.6–5.0 atomic%, respectively (Table 2). In contrast, both mainstream grains show Al (1.7 and 1.5 average atomic%), but no detectable Mg, implying upper limits of 0.08 and 0.18 atomic%, respectively. Some variation in the Al signal occurs across the mainstream grains, ranging from undetectable to 2.0 atomic%. No separate crystals of Al-bearing phases were detected, suggesting that the Al is heterogeneously distributed in solid solution, possibly in the form of AlN, which is isostructural to SiC. The Mg/Al ratios for the X grains range from 0.43–0.74. Relatively high Mg/Al ratios are commonly observed in SiC X grains (Nittler et al. 1995), as discussed in detail later (see the Trace Elements in Presolar SiC Grains section under Discussion). Of the two remaining X grains in this study, one contains no measurable Al or Mg, with upper limits of 0.7 and 0.2 atomic%, respectively, and the other grain contains measurable amounts of Al (1.3 atomic%), but no Mg. Both Al and Mg (when present) appear to be uniformly distributed within the X grains, although minor spot-to-spot variations of approximately 0.2% are observed. No other trace elements were observed in the grains.

## Grain Morphology and Crystal Domain Size

SiC is one of the hardest naturally occurring materials, so it tends to shatter when ultramicrotomed with a diamond knife. The breakage can be seen by comparing SEM (Fig. 3a) and TEM (Fig. 3b) images of the same grain. Despite this, ultramicrotomy does have the advantage of producing multiple slices for study, which sample the entire volume of the grain. In Fig. 3, the smaller diameter of the TEM slice compared to the whole grain is mainly due to sampling the grain off-center, although some material is also lost during slicing.

Each SiC X grain is observed to be an aggregate of many smaller SiC crystals. Although ultramicrotomy causes the SiC to have a fragmented appearance, it does not affect our ability to determine the crystal domain size or structure. Multiple crystal domains are observed within each fragment of an X grain slice (Figs. 4a and 4b). Since the crystal domains are smaller than the fragments, the fragmentation during ultramicrotomy does not result in an artificially small estimate of domain size. Six of the X grains are composed of crystals of similar size. Most of the domains are in the size range of approximately 100–200 nm, although each grain contained a few crystals that were larger than this range, as well as some smaller crystals. The total range in crystal size for these six grains is 56–457 nm, with a median geometric crystal diameter of 140 nm. A similar crystal domain size was observed by Stroud et al. (2004) in one of the two X grains they analyzed. The other X grain in this study (KJG-N4-185-1) had a much finer-grained appearance (Figs. 4c and 4d). This grain is

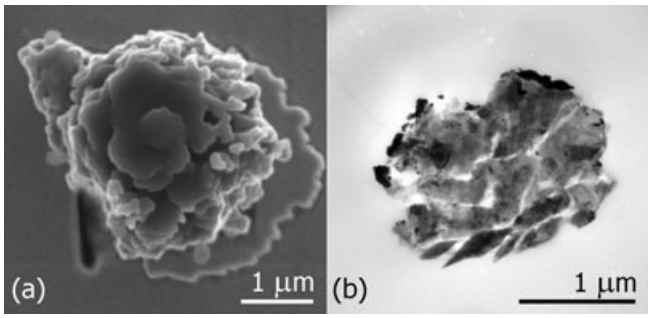


Fig. 3. a) SEM image of SiC X grain KJG-N4-585-2 after NanoSIMS analysis, but before slicing with the diamond ultramicrotome. b) Typical example of a grain after slicing. This bright-field (BF) TEM image shows one approximately 70 nm thick slice of the same grain pictured in (a). Although it has a broken appearance due to the slicing process, crystallographic properties are unaffected. Individual crystals are visible within the grain due to diffraction contrast and the black areas at the top edge of the slice are Au deposited during NanoSIMS analysis.

composed of much smaller crystals than the other X grains, with crystal domains that range from 24–135 nm, and a median diameter of 51 nm. Despite its different crystal domain size, the isotopic and elemental compositions of this grain are typical for X grains and not significantly different from the other X grains in this study. The second grain in the Stroud et al. (2004) study has smaller crystal domain sizes (approximately 10 nm crystals) than any of the X grains observed in this study.

Most previous TEM work on mainstream SiC has been done on relatively small grains (Daulton et al. 2003) that are 180–390 nm in diameter and are primarily composed of single crystals (66.4% of the population), although at least one grain larger than 1 μm has also been observed to be a single crystal (Stroud and Bernatowicz 2005). Because the bulk of previously analyzed presolar SiC grains are much smaller than the approximately 3 μm SiC X grains analyzed in this study, interpretation of the differences in crystal domain sizes between studies is problematic. Moreover, both trace element abundances (Amari et al. 1995) and the abundance of SiC grains from different types of stellar sources (Hoppe et al. 1996; Zinner et al. 2007) have been observed to vary systematically with grain size. Therefore, the observed differences in crystal domain sizes between the X grains in this study and the mainstream grains in the Daulton et al. (2003) study could be the result of analyzing two different SiC size fractions and not a result of the different stellar formation environments of mainstream SiC and X grains (AGB stars and SN outflows, respectively).

To facilitate a direct comparison with the X grains in this study, mainstream SiC grains from the same

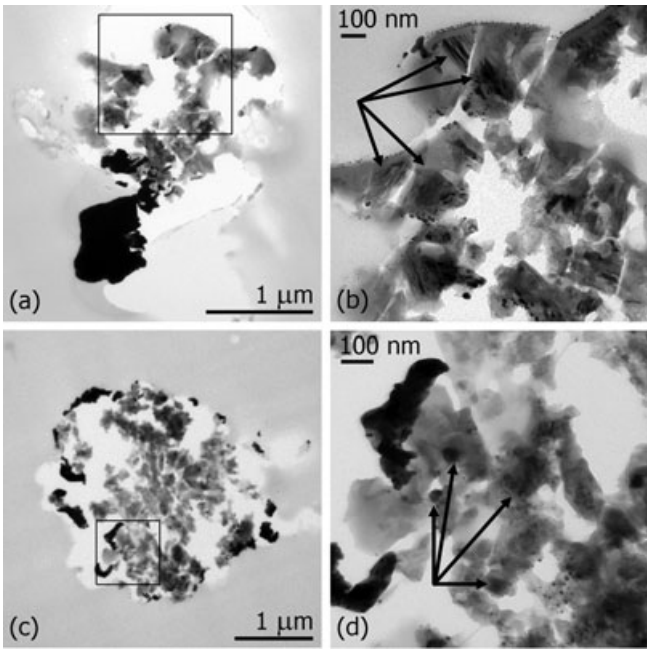


Fig. 4. TEM BF images of SiC X grains and their crystal domain sizes. a) The crystal domains (140 nm median diameter) observed in SiC X grain KJG-N2-411-2 are typical of six of the seven X grains. b) Individual crystal domains (examples indicated by arrows) are visible within the broken fragments of the grain in this magnified view (shown at $10^5 \times$ magnification) of the area indicated by a box in (a). Intensity variations between domains are due to orientation-dependent diffraction contrast. c) Grain KJG-N4-185-1 is composed of much smaller crystal domains (51 nm median diameter) than the other X grains. The smaller crystal domain size is visible in this image of the entire slice. d) Magnified view (at $1.2 \times 10^5 \times$ magnification) of the area indicated by a box in (c) showing individual crystal domains (examples indicated by arrows).

Murchison size fraction (KJG) as the X grains were analyzed for their crystal domain size and structure. The mainstream grains are also broken into several pieces as a result of ultramicrotomy, but unlike the X grains, no small crystals are visible within the fragments. To determine if each fragment is a separate crystal domain or if it is part of a larger crystal that had been shattered during slicing, a CBED pattern was obtained from a low index zone of one of the grain fragments. The grain was then tilted over an approximately 5° range around both axes of the sample stage goniometer to locate a nearby zone axis for each adjacent fragment. In this way, a CBED pattern was obtained for each fragment of the grain. The diffraction patterns were then analyzed to determine the polytype and crystal orientation of each fragment. Ideally, if the grain were a single crystal, at any given goniometer angle each fragment would be at the same crystallographic orientation. In reality, some minor

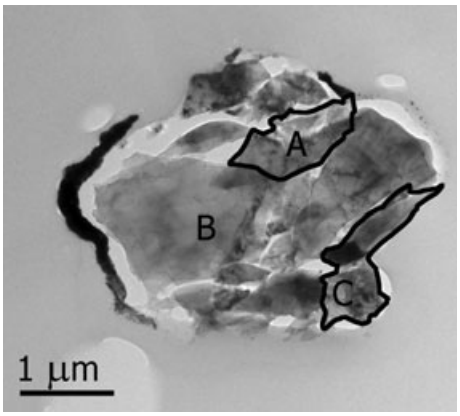


Fig. 5. TEM BF image of mainstream grain KJG-N4-595-1. Although the grains were broken into several pieces, the mainstream grains were actually composed of only 2–3 crystals. The three crystal domains observed in the grain are indicated by the letters A–C; the outlined areas (A and C) show the two smaller crystal domains and the remaining part of the grain (B) is the larger third domain.

displacement and rotation of the fragments occurs during ultramicrotomy, resulting in adjacent fragments having the same zone axis located at slightly different goniometer angles (a few degrees apart).

An example of this analysis is shown in Fig. 5, in which all of the fragments in mainstream grain KJG-N4-595-1 were indexed to either the [−112], [011], or [013] zone axes (of the 3C-SiC polytype), all found within approximately 8° of one another. In a single crystal, the angles of separation between <112> and <011>, <112> and <013>, and <011> and <013> zones are never less than 30°, 25.4°, and 26.6°, respectively. Since the zones in this grain are observed with smaller relative rotations (≤8°), the SiC grain in Fig. 5 must therefore be comprised of three separate crystal domains.

Utilizing this method, it was determined that both mainstream grains are composed of only a few large crystals. Grain KJG-N4-439-2 contains two crystal domains and the other, described above, contains three crystal domains. The crystal domains range in size from 0.5–1.7 μm. Because some material was probably lost during slicing, this is a lower limit on the domain size of these grains.

## Polytype Identification of KJG SiC Grains

The crystal structure was determined for each SiC grain, mainly with CBED patterns. Kikuchi bands were observed while tilting around both axes of the sample stage goniometer and used as a guide to locate low-index zones. In this way, several zone axes were located for each of the crystal domains analyzed. The <011> zones were used primarily for 3C-SiC polytype identification since these zone diffraction patterns are distinct from any formed by hexagonal or rhombohedral polytypes.

Due to the small crystal size of each SiC X grain (140 nm median crystal domain size for six grains, 51 nm for one grain), it is extremely difficult to analyze every crystal domain within each SiC X grain. Therefore, between five and eleven crystal domains were randomly selected from each grain for analysis for most of the grains. Unfortunately, only three crystal domains were available to be analyzed for two of the grains: one of which had only a limited area available for analysis and one in which the grid support failed. All but one of the crystal domains analyzed are of the 3C polytype (see below). This is also the most commonly observed polytype in mainstream grains (79.4% by number) (Daulton et al. 2003) and was also previously observed in one X grain (Stroud et al. 2004).

Polytype identification of many of these crystals was complicated by the presence of additional diffraction spots in <011> zones, indicating twinning. In the Daulton et al. (2003) study, the one third of SiC grains that are not single crystals are twinned. Twinning is the most common type of grain boundary in many cubic materials (see Daulton et al. 2003). It occurs across close-packed tetrahedral planes when a stacking fault suddenly reverses the stacking sequence of the SiC crystal and creates a mirror image of itself. A first-order coherent twin boundary is formed for a <011> zone when a stacking fault creates a rotation of 70.53° (plus an additional 180° to align the C-Si bonds) around an axis perpendicular to a {111} plane. Because bond lengths and angles are not changed, a low-energy interface results (Miura et al. 1990). All twinned crystals in this study and more than 95% of the twinned grains in the Daulton et al. study were of this type (the remaining approximately 5% in the Daulton et al. [2003] study were higher-order twins, which can result from rotations around axes perpendicular to {011} planes). First-order twinning is observable in a <011> diffraction pattern as a dimmer extra spot located at an interval of 1/3 along the spots caused by one {111} plane (Fig. 6b). This additional spot is caused by an extra reflection that arises from plural scattering from the twinned domain, which also normally contains less material than the matrix, and thus has a lesser intensity (Bender et al. 1986). Although the crystal has four unique {111} planes, twinning is only resolvable in <011> zones along the two planes with interfaces parallel to the electron beam (for a more extended discussion, see Bender et al. 1986).

In this study, six of seven X grains show first-order twinning along one of the sets of {111} planes. It is

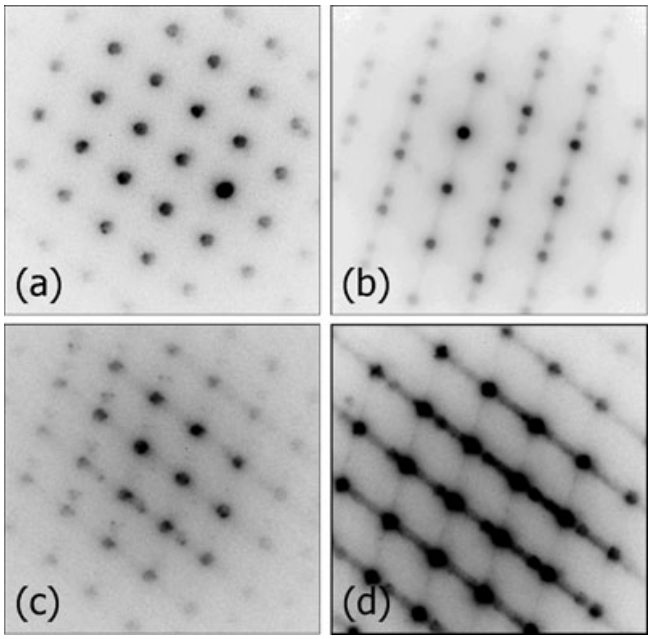


Fig. 6. Diffraction patterns of [011] zones showing examples of twinning along the {111} plane in SiC X grains (b–d) and an untwinned [011] diffraction pattern from a crystal domain in KJG-N4-585-2 for comparison (a). b) Extra spots are visible at intervals of 1/3 in this diffraction pattern from a crystal domain in KJG-N2-253-2, indicating a twin boundary. Twinning was observed in approximately 33% of SiC X grains. c) Extra diffraction spots are visible at intervals of 1/3 in two directions when a crystal is twinned along both possible {111} planes, as is the case for this crystal domain in KJG-N4-585-2. d) Streaking can also occur along twinned {111} planes, as seen in this pattern from KJG-N2-129-1.

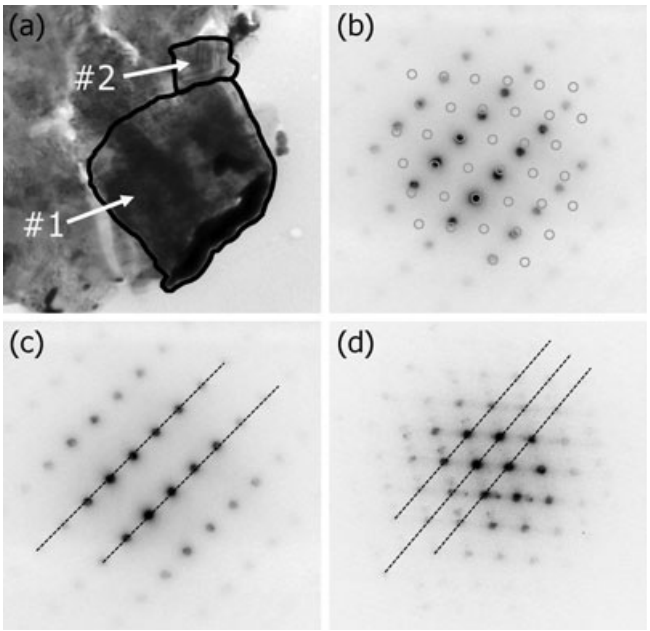


Fig. 7. Diffraction patterns at similar goniometer angles from two neighboring crystals were obtained from X grain KJG-N4-585-2 (a). A [−112] diffraction pattern was obtained from crystal #1 (c) and a [011] pattern from crystal #2 (d). The epitaxial growth of these two crystals is evident in (b) when pattern (d) is overlaid onto pattern (c). For clarity, the spots in the [011] pattern are drawn as empty gray circles. The (1-11) and (200) planes of the [−112] and [011] zones respectively are almost perfectly aligned (with a 4° mismatch), indicating epitaxial growth. These planes are indicated with a dashed line in figures (c) and (d). Other adjacent crystals have similarly closely aligned planes, with most mismatches varying from approximately 2°–4.5°.

possible that the seventh X grain (KJG-N4-263-1) was also composed of twinned crystals, but none were observed due to the small number of crystal domains available for study in this grain. Approximately one-third of the crystals analyzed are twinned, but this is clearly a lower limit since only two of four unique {111} planes that could potentially show twinning lie within the tilt limits of the TEM goniometer. To confirm the twin identification, diffraction patterns from another $<011>$ zone (located 60° away in tilt from the original $<011>$ twin boundary zone) were obtained from each side of the twin boundary. These patterns are rotated 70.5° from one another, providing conclusive evidence of a twinned 3C-SiC structure. Only one crystal showed twinning along both {111} planes (Fig. 6c). Some crystals also show streaking along the {111} planes, indicating stacking faults in this direction (Fig. 6d). The precise orientation relationship required for a twinned structured is further evidence that the observed small crystal domain sizes in X grains are not a result of ultramicrotome damage. If larger crystals were simply broken apart during slicing (as it appears for the mainstream grains), then it is highly improbable that the crystals would still display the same crystallographic twinning relationships that they do.

In order to further investigate the relationship between crystal domains in SiC X grains, CBED patterns were obtained at similar sample orientations for low index zones from neighboring crystal domains in an unbroken portion of an X grain. Analysis of these diffraction patterns indicated that neighboring crystal domains share a common growth plane. An example can be seen in Fig. 7. For the crystal domains thus analyzed, a mismatch of 1.7°–7°, with all but one crystal domain aligned within 4.4°, was observed, clearly indicating an epitaxial relationship between neighboring crystal domains. For groups of neighboring crystal domains in other grains, similarly well-aligned planes were observed. This close alignment would be extremely unlikely if the crystals grew independently and then randomly coalesced into a mechanical aggregate.

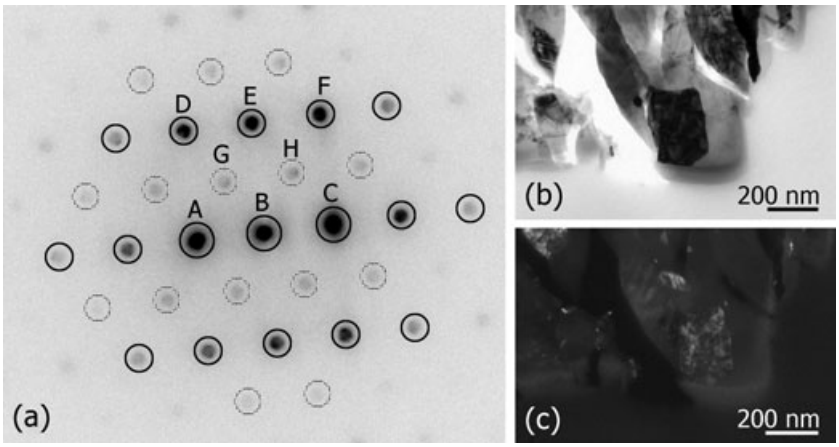


Fig. 8. A diffraction pattern (a) from one crystal in SiC X grain KJG-N2-31-1 shows an intergrowth between the 3C-SiC and 2H-SiC polytypes. The dark spots (indicated by solid circles) index to both the [112] zone of 3C-SiC and the [0001] zone of 2H-SiC. These spots are shared by the {10-10} plane of 2H-SiC and the {11-1} plane of 3C-SiC. The minor difference in d-spacings between the 2H-SiC {10-10} and 3C-SiC {11-1} diffraction spots (nominally 6%) is not seen. The lighter spots (indicated by broken circles) index to only the [0001] zone of 2H-SiC. The letters above some of the spots represent indexing of the diffraction spots that correspond to: $A$ = (-1-10)/(-1010) spots; $B$ = (000)/(0000); $C$ = (11-1)/(10-10); $D$ = (-311)/(-2200); $E$ = (-220)/(-12-10); $F$ = (-13-1)/(02-20); $G$ = (-1100); and $H$ = (01-10). Comparison of a BF image (b) and a DF image (c) (taken with the diffraction spot indicated by "H") shows signal emanating from the entire crystal, while additional diffraction patterns indicate the entire crystal is 3C-SiC. This suggests a close intergrowth of the two polytypes instead of distinct domains of the crystal for each polytype.

Only one grain contains a crystal domain that does not index to the 3C polytype; this was found in grain KJG-N2-31-1 and appears to be an intergrowth of the 3C and 2H polytypes (Fig. 8). A [112] diffraction pattern from this crystal domain also contains extra, lighter rows of spots between the (11-1) planes of the [112] zone. The spacing of these extra spots is inconsistent with twinning or another 3C-SiC domain. Instead, the extra pattern indexes to the [0001] zone of the 2H-SiC polytype. The {11-1} spots of the [112] 3C-SiC pattern are aligned with the {10-10} spots of the [0001] 2H-SiC zone, indicating an intergrowth. Additional diffraction patterns from this crystal indicate that it is predominantly 3C-SiC, but dark field (DF) images obtained from diffraction spots unique to the 2H-SiC polytype show a signal emanating from the entire grain, indicating the 2H-SiC intergrowth occurs throughout the grain as well. This suggests a close intergrowth between the two polytypes that switches back and forth between the two throughout the grain. No streaking or additional spots are evident in any of the other 3C-SiC patterns obtained from this crystal. Although intergrowths between the 3C and 2H polytypes have not been previously reported in X grains, they occurred in approximately 17% of the grains in the Daulton et al. (2003) study. However, unlike the X grain crystal domains in the present study, their grains were composed of a distinct crystal domain for each polytype, with the proportion of 2H-SiC to 3C-SiC varying greatly between grains, from primarily 3C-SiC to primarily 2H-SiC.

Unlike the small crystal domains in SiC X grains, each SiC mainstream grain section is only broken into approximately 10–15 fragments. Zone axes were located for each fragment in the two mainstream grains. All the fragments were conclusively indexed to the 3C polytype. Although each grain is composed of several crystal domains, the grain, as a whole, is a single polytype. In this study, limited crystallographic information was obtained for the mainstream grains, as they were analyzed primarily to provide a comparison to the crystal domain size of the X grains of comparable total grain size (approximately 3 μm). The reader is referred to Daulton et al. (2003) for additional crystallographic information on SiC mainstream grains.

### Internal Grains within SiC X Grains

Eight internal subgrains were identified in a total of two X grains, making them the first subgrains identified in SiC X grains (Hynes et al. 2006). Seven of the eight subgrains were identified in grain KJG-N2-129-1 (Fig. 9a). The internal grains, as well as their relative positions within the SiC grain, are shown in Figs. 9a–e, and their sizes and compositional information are listed in Table 3. All of the grains are located within a single slice of KJG-N2-129-1 and five of the grains are clustered in a small area approximately 200 nm in

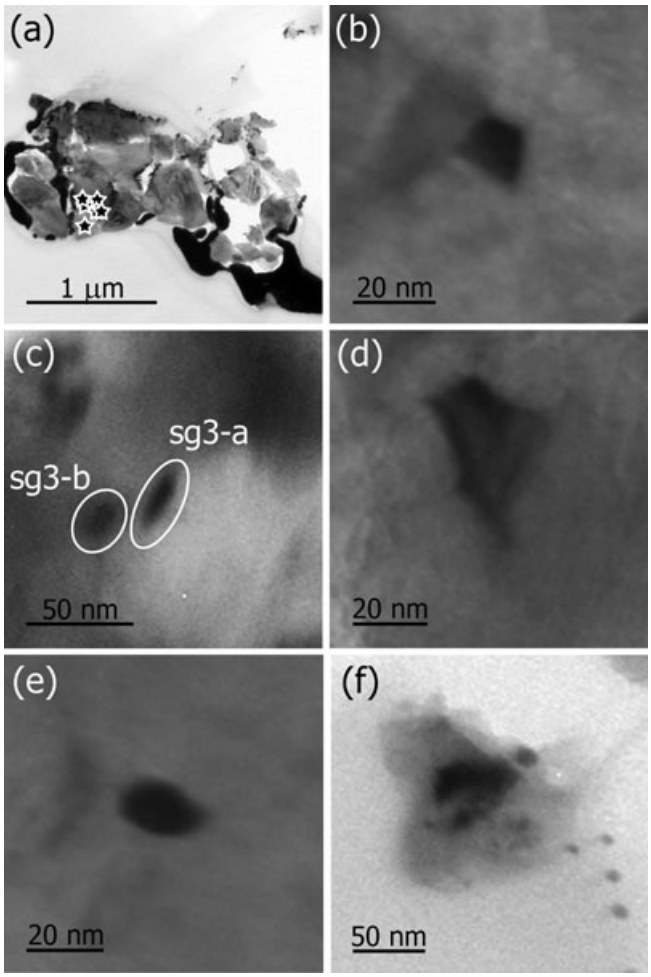


Fig. 9. TEM BF images of four of the seven internal subgrains in KJG-N2-129-1 (b–e) and one subgrain in KJG-N4-185-1 (f). The internal subgrains in KJG-N2-129-1 are all localized in an area of a few hundred nanometers in the grain. The location of each of these subgrains is indicated by a star in (a). Subgrains 3-a and 3-b are only a few nanometers apart from one another and are therefore indicated with a single star. The subgrains pictured are: from KJG-N2-129-1, sg1 (b); sg3a and sg3b (c); sg4 (d); sg5 (e); and from KJG-N4-185-1 sg1 (f).

diameter; only sg3-a and sg3-b are located approximately 500 nm away from the others. The subgrains are all relatively small, ranging in size from 11–45 nm. They are, however, only slightly smaller than some of the SiC crystal domains. The morphology of the subgrains is euhedral to subhedral, with growth faces clearly visible. Only a single subgrain is located in KJG-N4-185-1 (Fig. 9f), but the extremely small crystal domain size of this grain made it difficult to locate subgrains in this SiC. Despite the smaller SiC domain size of grain KJG-N4-185-1 compared to the other SiC X grains, its internal grain is of a similar size to those found in KJG-N2-129-1. However, the subgrain appears to be subhedral compared to those in KJG-N2-129-1.

Table 3. Summary of internal subgrains within SiC X grains.

| Grain label | Subgrain label | Size (nm) | Ni/Fe[a] | Ti/Fe[a] |
|---|---|---|---|---|
| KJG-N2-129-1 | sg1 | 18 × 13 | 1.60 | |
| KJG-N2-129-1 | sg2 | 44 × 29 | 0.18 | |
| KJG-N2-129-1 | sg3-a[b] | 45 × 22 | 0.34 | 3.15 |
| KJG-N2-129-1 | sg3-b[b] | 26 × 15 | 0.12 | < 0.1 |
| KJG-N2-129-1 | sg4 | 33 × 21 | 0.40 | |
| KJG-N2-129-1 | sg5 | 23 × 11 | 0.41 | |
| KJG-N2-129-1 | sg6 | 40 × 37 | 0.18 | |
| KJG-N4-185-1 | sg1 | 28 × 50 | 1.61 | |

Notes: [a]Due to the small size of the grains, all Ni/Fe and Ti/Fe ratios have large errors of 5–10%.
[b]Subgrain was originally labeled as sg3, but appears to be composed of two unique pieces: sg3-a and sg3-b. Due to their proximity, some signal overlap may occur.

EDXS analysis indicates that all but one of the eight internal grains are composed of only Fe and Ni (in addition to the elements present in the surrounding SiC). The Ni/Fe ratios are highly variable, ranging over almost an order of magnitude from 0.18–1.61 (Table 3). Unfortunately, these subgrains are probably too small to be analyzed in the NanoSIMS to determine their isotopic composition. Only sg3 in KJG-N2-129-1 has detectable amounts of another element. This subgrain contains significant amounts of Ti. While the subgrain at first appeared to be a single crystal, a more detailed examination revealed the subgrain to actually be two subgrains. Although some of the EDXS signal likely overlapped between the two pieces of sg3 (sg3-a and sg3-b), they have detectably different compositions, with sg3-a containing nearly all of the Ti and sg3-b containing almost none, which is compositionally consistent with a TiC subgrain with an attached metal phase. Both portions of sg3 are Fe-rich, although sg3-b contains significantly more total Fe than sg3-a. Unfortunately, due to failure of the support substrate, crystallographic information could not be obtained for these subgrains to further identify them and clarify their relationship.

Diffraction patterns were obtained from the rest of the subgrains in KJG-N2-129-1, as well as from the adjacent SiC crystals. Utilizing the known d-spacings from the SiC crystals as calibration, the d-spacings and interplanar angles from the subgrains' diffraction patterns were calculated. The d-spacings from at least one diffraction pattern for each of the subgrains are too large by 22–29% to be kamacite (bcc; $a$ = 2.87 Å) and by 18–25% to be taenite (fcc; $a$ = 3.60 Å), which are the only Fe-Ni metal phases previously observed in carbonaceous presolar grains (Croat et al. 2003). An accuracy of better than approximately 5% is expected with the internal calibrations, clearly indicating that the

subgrains are a different phase than any previously observed. Further analysis showed that all the subgrains are inconsistent with any purely metallic Fe-Ni phase. Possible minerals are also limited by the EDXS composition. Given that the sizes of the subgrains are less than the thickness of an ultramicrotome slice, significant EDXS contributions from the SiC matrix are unavoidable. For this reason, the C and Si elemental content of the subgrains cannot be determined, since the strength of these elemental peaks depends on the relative contribution from the SiC background, which varies greatly depending on subgrain size, TEM beam orientation, and other factors. However, the relative strength of the O peak did not change when measuring the subgrain versus the bulk SiC, indicating that the O is just background signal, and eliminating oxides and silicates as possible candidates. Comparison of the d-spacings and the interplanar angles from the subgrains' diffraction patterns were used to further rule out carbides, nitrides, and minerals containing Al and Mg. Silicides [e.g., $(Fe, Ni)_3Si$, $(Fe,Ni)_2Si$], however, are good candidates that match the diffraction patterns and d-spacings of the subgrains. The diffraction data for all of the subgrains are consistent with a silicide identification. Silicides also have a broad range of compositions, widely varying in both Ni/Fe and metal to Si ratios. However, with a limited number of subgrain candidates, it is difficult to conclusively determine the stoichiometry and crystal structure of the silicides that are present in SiC X grains. Due to the large compositional range, large crystal lattices, and similar diffraction patterns produced by many silicides [e.g., $(Fe, Ni)_3Si$; monoclinic; $a$ = 6.972 Å, $b$ = 6.254 Å, $c$ = 7.656 Å, β = 87.75° and $(Fe,Ni)_2Si$; orthorhombic; $a$ = 3.73 Å, $b$ = 5.00 Å, $c$ = 7.04 Å], several silicide compositions can match the data from a single subgrain.

## DISCUSSION

### Trace Elements in Presolar SiC Grains

One of the definitive characteristics of SiC X grains is their high level of radiogenic $^{26}Mg$ from the decay of $^{26}Al$ (half-life = $7.4 \times 10^5$ yr), which is synthesized mainly in SNe, although smaller amounts can also be produced in AGB stars. The $^{26}Mg$ is assumed to be radiogenic for both chemical and isotopic reasons. First, Al preferentially condenses into SiC, giving Al/Si ratios of up to several weight percent in both SiC X grains and mainstream grains (Hoppe and Ott 1997). However, unlike Al, Mg does not readily condense into SiC, leading to typical concentrations in mainstream SiC grains of only approximately 100 ppm (Amari et al. 1995). Presolar SiC grains have isotopically normal $^{25}Mg/^{24}Mg$ compositions, but show enrichments in $^{26}Mg$, further supporting the idea that the bulk of the $^{26}Mg$ measured in presolar SiC grains is due to the decay of $^{26}Al$. Based on this assumption, the inferred initial $^{26}Al/^{27}Al$ ratio can be calculated from Mg isotopic data. The inferred $^{26}Al/^{27}Al$ ratios for SiC mainstream grains are typically very low (approximately $10^{-3}$–$10^{-4}$) (Hynes and Gyngard 2009), with correspondingly low Mg/Al ratios ($< 0.05$) (Amari et al. 1995). SiC X grains, however, have much higher inferred $^{26}Al/^{27}Al$ ratios (approximately $10^{-2}$–$10^{-1}$) (Hynes and Gyngard 2009), ranging as high as 0.6 (Nittler et al. 1995).

Our EDXS data are consistent with previous isotopic findings. The mainstream grains do not show any measurable Mg, while most of the X grains have very high Mg/Al ratios (up to 0.74). With such low Mg concentrations in mainstream grains (in both TEM and isotopic measurements) and the $^{26}Mg$ excesses measured in presolar SiC grains generally being very high, with sometimes even monoisotopic $^{26}Mg$ (Hoppe and Ott 1997), it is possible to estimate the inferred $^{26}Al/^{27}Al$ isotopic ratios from elemental Mg/Al ratios. Within a $2\sigma$ error, the $^{26}Al/^{27}Al$ ratios inferred from our Mg/Al elemental ratios are consistent with the $^{26}Al/^{27}Al$ ratios inferred from isotopic data: $< 0.12$ to $0.74 \pm 0.04$ and $0.003 \pm 0.002$ to $0.61 \pm 0.04$, respectively.

The Al in SiC grains has been postulated to be in the form of AlN, an idea that has been supported by TEM observations of AlN subgrains in a SiC mainstream and Z grain (Stroud and Bernatowicz 2005). Materials science research indicates that the solubility of AlN in solid solution varies with SiC polytype. Aluminum was found to be most soluble in 2H-SiC and extremely insoluble in 3C-SiC (Zangvil and Ruh 1988). Contrary to these findings, there is no obvious difference between Al-Mg content and polytype evident in this study; in fact, the only SiC grain indexed to 2H-SiC (grain KJG-N2-31-1, an intergrowth between the 3C and 2H polytypes) contains some of the lowest Al-Mg concentrations. Unfortunately, to the best of our knowledge, measurements of Al-Mg concentrations in presolar grains with coordinated crystallographic analyses are only available for the grains in this study. Additional Al-Mg measurements on grains with the 2H polytype are needed to determine if Al content in presolar SiC grains is correlated with polytype.

### Effects of Stellar Environment on Grain Formation and Crystal Growth

The SiC X grains and mainstream grains were observed to have significantly different crystal domain

sizes. SiC X grains, both from this study and from previous studies, are polycrystalline, even X grains that are submicron (Stroud et al. 2004), whereas mainstream grains are either single crystals (Daulton et al. 2003; Stroud and Bernatowicz 2005) or composed of only a few large crystals. In this study, the crystal domains in the mainstream grains range from several times to over 30 times larger than those in the X grains. The difference can be explained as resulting from the different environments in which these grains formed. The large number of crystals in each SiC X grain implies a large number of nucleation sites, which in turn suggests conditions of high supersaturation in the parent gas. If the gas is not supersaturated, small condensation nuclei that form will quickly redisperse due to free energy constraints because the free energy of a seed nucleus is higher than that of the bulk gas. However, crystallites will form and reach critical size under conditions of supersaturation. These conditions foster both rapid nucleation and growth, with new crystallites nucleating at the expense of the growth of other crystals, resulting in many small crystals growing together into a single grain, as was observed in the X grains. Lower degrees of supersaturation would lead to lower nucleation rates and increased growth, producing fewer, but larger crystals within a single grain, as was observed with the mainstream grains.

It is useful to compare these growth scenarios to previous theoretical and experimental works on the growth conditions around AGB stars and SN outflows. An origin in the envelopes of low-mass carbon AGB stars has been well established for mainstream SiC, as well as for some graphite grains (Bernatowicz et al. 1996; Meyer and Zinner 2006). Bernatowicz et al. (2005) sought to determine the physical conditions, including stellar mass and timescale, required to form micron-size presolar graphite grains and their internal TiC subgrains in the outflows of AGB stars, beginning with the fundamental idea that in order for stars to contribute to the presolar grain population, they must have sufficient mass to reach the AGB phase soon enough to contribute dust to the solar nebula. The resulting mass limit excludes hot carbon stars, leaving carbon variable (CV) stars, which have radii, luminosities, and effective temperatures that vary periodically with time, as the likely source of presolar SiC and graphite with an AGB origin. Using equilibrium thermodynamics calculations and kinematics, as well as mass-loss rates and outflow velocities of CV stars from astronomical observations, they determined the radii at which the grains would form and the effective temperatures at which grain growth would begin and cease. With these parameters, they calculated a time interval (governed largely by the range of the luminosities of CV stars) of approximately 2–10 yr during which graphite growth could occur. This timescale begins with nucleation and ends when the number density in the gas drops so low that grain growth effectively ceases. These calculations were done for graphite and TiC, but they can be adapted for SiC. Grain growth largely depends on the number density of each species and is therefore limited by the less abundant species. The solar ratio of Si/C is 0.14, but when only free C is considered (C not tied up in CO molecules and thus free to form carbonaceous grains), for C/O ratios of 1.05–1.15, the ratio of Si/C ranges from 1.42–0.47 (Lodders 2003). At a C/O ratio of 1.05, the formation of graphite and SiC remove roughly the same amount of C from the total C (Lodders and Fegley 1995), suggesting that both SiC and graphite will continue to grow over similar timescales.

A timescale for the formation of SiC X grains in SN ejecta has also been estimated. Hoppe and Besmehn (2002) measured the Ti and V isotopic compositions of SiC X grains. The radioactive isotope $^{49}$V (half-life = 338 days) is produced from the decay of $^{49}$Cr (half-life = 42 min) by explosive Si, O, and He burning in the Si/S and Ni zones of a SN (Meyer et al. 1995). Vanadium-49 then decays into $^{49}$Ti, which allows a timescale for grain formation to be estimated. If the time of formation were much longer than the half-life of $^{49}$V, it would have decayed into $^{49}$Ti before its incorporation into the SiC grain and resulted in no correlation between Ti and V (measured as $^{49}$Ti/$^{48}$Ti and $^{51}$V/$^{48}$Ti). If, however, the formation timescale were shorter than the half-life of $^{49}$V, live $^{49}$V would be incorporated into the grains and subsequently decay into $^{49}$Ti, resulting in a correlation between Ti and V. Hoppe and Besmehn (2002) found a positive correlation between $^{49}$Ti/$^{48}$Ti and $^{51}$V/$^{48}$Ti, suggesting that the $^{49}$Ti excesses are due to the incorporation of live $^{49}$V into the X grains. Additionally, $^{46,47,50}$Ti/$^{48}$Ti were close to solar values. The presence of live $^{49}$V during grain formation led them to calculate that the timescale for SiC X grain formation was a period of months, and with uncertainties included, no more than 25 months. This timescale begins with the SN explosion (and the creation of $^{49}$V) and ends when grain growth effectively ceases. However, grain formation does not begin with the SN explosion, in which temperatures reach approximately $5 \times 10^5$ K and all surrounding material is vaporized (Wooden 1997); this timescale estimate does not take into account the time necessary for the ejecta to cool enough for grains to condense. Although astronomical observations of dust around Type II SNe are limited, SN 1987A had strong infrared emissions, indicating the onset of dust condensation between approximately 350–500 days after the explosion (Wooden 1997). Although the dust emission was

dominated by grains with featureless spectra, such as metallic C and Fe grains, the timescale for dust formation agrees with that predicted by Hoppe and Besmehn (2002). However, their estimated timescale is an upper limit on the time available for X grain formation, particularly if grain formation does not begin until approximately 500 days after the SN explosion, suggesting that the actual time for grains to form may be less than a year.

The total size to which a SiC grain can grow is directly proportional to both the growth timescale and the average total pressure, which affects the availability of condensable species. In SN ejecta, these conditions vary rapidly. The explosion itself is incredibly powerful, releasing approximately $10^{46}$ J of energy. The gas then rapidly expands, with initial speeds of (4–30) $\times$ $10^3$ km $s^{-1}$, and quickly cools; observations of SN 1987A indicate that the temperature drops from approximately 500,000 K to ≤2000 K in only 350 days, with a corresponding decrease in pressure (Wooden 1997). The radioactive decay of isotopes like $^{56}$Ni heats the ejecta, while instabilities, such as high temperature Rayleigh-Taylor fingers, create turbulent mixing throughout the SN ejecta. In this rapidly evolving environment, SiC X grains are thought to condense. High initial pressure, which ultimately leads to the growth of large grains, coupled with sharp drops in pressure and rapid cooling would favor supersaturation with rapid and prolific nucleation and crystal growth, in agreement with the large number of crystal domains observed in X grains. This is also consistent with astronomical observations of SN 1987A, in which dust condensation occurred rapidly enough to fill 50% of the ejecta volume after just 500 days (Wooden 1997). With the short timescale available for X grain growth suggested by both astronomical observations (Wooden 1997) and isotopic measurements (Hoppe and Besmehn 2002), each individual crystal domain does not have time to grow very large before being encroached upon by adjacent growing crystal domains, resulting in many small crystal domains in a single SiC X grain, consistent with the observations in this study. The conditions in the AGB outflows in which SiC mainstream grains condense, however, are quite different. Pressures and temperatures remain relatively constant. Although temperatures and pressures typically are approximately 2000–2500 K and approximately 100 N/$m^2$ in the photosphere of an AGB star, these temperatures are far too high for grain condensation to occur. At larger radii where SiC grains can condense, temperatures (approximately 1400–1700 K) and pressures (roughly 0.01–10 N/$m^2$) are much lower (Lodders and Fegley 1995). Under these conditions, nucleation would occur at a slower rate than in SN ejecta and would result in fewer nucleation sites. However, some variation in condensation conditions in AGB stars likely occurs throughout the period of grain growth and between individual stars, resulting in some mainstream grains being composed of a single crystal domain, while others are polycrystalline. In addition to slower nucleation in AGB stars, given the growth period of years for mainstream grains to grow in AGB outflows calculated by Bernatowicz et al. (2005), these crystals would have a significantly longer time to grow and to cool than their counterparts in SN outflows, resulting in relatively large, but few, crystal domains in each mainstream grain, also in agreement with the observations of this study. Therefore, both the timescale for grain formation and the nucleation rates lead to the growth of many small crystal domains in X grains, relative to mainstream grains with the same total grain size.

Based on the different grain formation conditions and environments in AGB stars and SNe, which are manifested in the different isotopic characteristics and different crystal domain sizes measured in mainstream SiC and X grains, it may seem plausible that these different environments would also be reflected in the presence of different polytypes in X grains and mainstream grains. However, the same polytypes have been observed to occur in both types of grains. Among the crystals in the X grains in this study and the two X grains analyzed by Stroud et al. (2004), examples of each polytype (3C and 2H) observed by the Daulton et al. (2003) study are found, with the exception of 1-D disordered grains, which are less than 1% by number of presolar SiC grains and thus statistically unlikely to be observed in either our study or the Stroud et al. (2004) study, although Daulton et al. (2009) have recently identified a 1-D disordered X grain.

Some insights into why only the 2H and 3C polytypes are observed in presolar grains can be gained by looking at the experimental and theoretical work done on the conditions that affect SiC polytype growth in general. Due to the usefulness of SiC as a wide band gap semiconductor that can be used in hostile environments, it has found many uses in aerospace and defense applications, and even as coatings on very high temperature nuclear field reactors. Because some polytypes of SiC are better suited than others for wide ranging applications, considerable research has been done by the materials science community over the last 40 yrs to understand SiC formation and growth.

Despite much research on the subject, the theoretical details of the formation and growth of SiC polytypes are still not well understood and it is unclear what factors dominate formation in any individual case. Theories based on nucleation growth models and

experimental results suggest a wide variety of factors may play an important role in determining which polytype forms. These include: the influence of physical conditions, such as temperature, pressure, and the C-flux; the effect of the Si/C ratio in the gas; the growth surface or nucleation seed and its polarity; the presence of impurities; the location and number of stacking faults present; the effects of non-equilibrium conditions; the presence of vacancies in the superlattice; and the differences between polytypes in formation energy and surface free energy (see Fissel 2000; Zhaoqing and Jun 2005; and references therein). Experimental results are also varied and are highly dependent on experimental conditions. Different growth methods can lead to the formation of the same polytypes at very different temperatures and can result in different transitions from one polytype to another, with possible intergrowths occurring at intermediary temperatures. For example, SiC vapor was observed to first crystallize as 3C-SiC and then begin to transition to the 6H polytype at temperatures of approximately 2100–2700 K (Yoo and Matsunami 1991; Anikin and Madar 1997). Above 2700 K, the SiC gas condensed directly to 6H-SiC. The same transition was observed to occur at approximately 1620 K for SiC grown with gas-source molecular-beam epitaxy (Kern et al. 1998). The 3C polytype can also form via transformation of the 2H polytype by annealing in an Ar atmosphere at temperatures ranging from approximately 1673–1763 K (Krishna et al. 1971). In other experiments utilizing condensation of gaseous SiC onto graphite wafers, 2H-SiC was observed to start growing at temperatures approximately 1500 K and cease transitioning to 3C-SiC above approximately 1700 K (Patrick et al. 1966; Stan et al. 1994). In both vapor condensation and annealing experiments, the 2H to 3C to 6H-SiC transition has been frequently observed; however, 4H-SiC has also often been observed as an intermediary step after 3C-SiC. Both the 3C-SiC and 4H-SiC steps can also be omitted, resulting in a direct transition from 2H-SiC to 6H-SiC, even with techniques similar to those previously described. For example, 2H-SiC crystals, annealed in an Ar atmosphere, were observed to transition directly to 6H-SiC at 2673 K (Krishna and Marshall 1971).

Unfortunately, some difficulties arise in trying to apply the laboratory experimental conditions that result in a wide range of transitions and temperatures to the growth conditions in stars. No lab can accurately model the temperatures, pressures, gas-flux, growth surfaces, and possible non-equilibrium conditions present in SN outflows. Therefore, while laboratory experiments can provide a useful tool in understanding polytype formation, the exact temperatures of formation, conditions for possible intergrowth, and the transitions to higher-order polytypes are still uncertain.

However, despite large variations in temperatures, some general trends are clearly apparent. 2H-SiC is the lowest-order polytype that has been observed to form. Furthermore, only 2H-SiC has been observed at lower temperatures than 3C-SiC, marking 2H to 3C-SiC as the lowest temperature transition, with possible intergrowths between the two polytypes occurring at a range of intermediary temperatures. At even higher temperatures, both 2H-SiC and 3C-SiC become unstable and cease to form, resulting in gaseous SiC crystallizing directly into higher-order polytypes like 6H-SiC. Transitions from higher-order polytypes to lower order ones, such as 6H-SiC to 3C-SiC, have not, however, been observed.

Equilibrium condensation calculations for the formation of SiC and graphite suggest that grain formation is limited to pressures of 0.01–10 $N/m^2$ and C/O ratios of 1.05–1.2 (Lodders and Fegley 1995; Sharp and Wasserburg 1995). Under these conditions, SiC is expected to condense at temperatures of 1390–1630 K. Some SN models predict SiC formation at a similar, although slightly higher, temperature of 1745 K (Lattimer et al. 1978). The temperatures predicted for SiC grain formation in stellar outflows are roughly in line with experimental evidence for the growth of the lower temperature polytypes, i.e., 2H-SiC and 3C-SiC. Although approximately 250 higher-order hexagonal and rhombohedral polytypes have been observed to form in laboratories, they require high temperatures above approximately 2800 K (Fisher and Barnes 1990), far too high for SiC to condense, given the low pressures in stellar outflows. However, these condensation models assume the grains form near thermochemical equilibrium, which is likely to be true in AGB stars, but may not be true in SNe (Ebel and Grossman 2000).

The presence of only the 2H and 3C polytypes, or intergrowths of the two, in presolar SiC suggests two possible explanations. The first is that the conditions under which SiC starts to form may not be that different in AGB stars and SNe, despite the fact that SN outflows may initially have significantly higher temperatures and pressures than do AGB outflows (Lattimer et al. 1978; Sharp and Wasserburg 1995). The other possibility is that polytype formation is not particularly sensitive to these conditions, at least at the ranges present in both kinds of stellar outflows. Other factors, such as the Si/C ratio or the flux of C and Si onto growing particles, may play a more dominant role in polytype formation over the range of temperatures and pressures found in stellar ejecta and therefore contribute to the formation of the same polytypes in

both mainstream and X grains. The resolution of this question requires a better theoretical understanding of the fundamental factors that dominate SiC polytype formation. As a final caveat, the number of X grains that have been analyzed in the TEM, though much improved, is still reasonably small, especially in comparison to the hundreds of mainstream grains analyzed, e.g., by Daulton et al. (2003). In view of the somewhat limited sample size, it is still possible that higher-order polytypes may yet be discovered in SiC X grains.

While materials science experiments on polytype growth produce widely varying results, they agree with both this study and the Daulton et al. (2003) study that 3C-SiC is the preferred polytype at low temperatures. Daulton et al. (2003) suggested that the observed abundance of 3C-SiC over 2H-SiC can be explained for AGB stars by the formation of 2H-SiC at large circumstellar radii, where temperatures prevail that are low enough for only 2H-SiC to form. At smaller radii, the temperature would be high enough to allow for both the 2H and 3C polytypes to form, resulting in possible intergrowths between the two polytypes; at still smaller radii, even higher temperatures would cause 2H-SiC formation to cease, resulting in the formation of only 3C-SiC. The number densities are also higher at smaller radii, resulting in more 3C-SiC relative to 2H-SiC. In addition, more of the Si will have already condensed as 3C-SiC at smaller radii, resulting in fewer intergrowths and even less of the 2H-SiC polytype.

However, the observed preponderance of 3C-SiC is in stark contrast to nucleation theory, which predicts that 3C-SiC is never the stable polytype of SiC at any temperature. 3C-SiC has both a much higher total lattice energy (an important theoretical constraint on polytype formation) and a higher phonon energy (which is thought to stabilize polytypes by contributing to the free energy) than both 4H-SiC and 6H-SiC (Zhaoqing and Jun 2005). Of the most common polytypes, only 2H-SiC is less energetically favorable than 3C-SiC. However, the frequent experimental observations of 3C-SiC at low temperatures can be explained by its propensity to grow epitaxially (a phenomenon that was also observed in the formation of X grain aggregates in this study). SiC vapor growth can be viewed as a layer-by-layer process in which a single Si-C bilayer at a time is added to the crystal. At high temperatures, with each new bilayer, the crystal can rearrange itself to create the most energetically favorable stacking sequence, resulting in either 4H-SiC or 6H-SiC. However, at lower temperatures, the crystal is unable to reorient the already formed layers and must simply arrange the newest layer into a locally energetically favorable stacking, which results in the 3C polytype (Heine et al. 1991). This should also be the case far from equilibrium, where rearrangement of the Si-C bilayers is not possible (Fissel 2000). The composition of the gas from which the SiC grains condense has also been shown to affect polytype formation. 3C-SiC has been both theoretically predicted and experimentally observed to preferentially form over any other polytype at temperatures $< 2000$ K (at which 3C-SiC, 4H-SiC, and 6H-SiC have all been observed to form in a laboratory setting) under conditions of supersaturation of the C-flux and high Si/C ratios. However, at lower C-fluxes and Si/C ratios, 6H-SiC was observed to form and at still lower Si/C ratios, 4H-SiC formed (Fissel 2000). No clear theoretical reasons exist to explain the observed formation of 2H-SiC and the transition of 2H-SiC into 3C-SiC (Krishna et al. 1971) other than temperature constraints (Fissel 2000). Although the applicability of laboratory experiments and nucleation theory has some limitations, until a more complete theory of polytype formation is developed, they provide possible scenarios for the observed polytype abundances in SiC X grains.

### Subgrain Formation in Stellar Outflows

While not previously observed in SiC X grains, subgrains are quite common in carbonaceous presolar grains. Although a limited number of SiC grains have been sectioned for TEM analysis, subgrains have been found within four of eight presolar SiC grains studied (Bernatowicz et al. 1992; Stroud and Nittler 2004; R. Stroud, personal communication). Bernatowicz et al. (1992) observed TiC subgrains in a mainstream SiC grain. (Ti,V)C was also observed in two different pristine SiC grains, along with AlN subgrains, by Stroud and Bernatowicz (2005). Finally, multiple graphite subgrains in SiC were observed by Stroud et al. (2002). All of these SiC grains originated in an AGB circumstellar environment.

Subgrains are also quite common in presolar graphite grains. Approximately 20% of the roughly 850 high-density graphite slices analyzed by Croat et al. (2005) contain subgrains. Most of these grains are (Ti, Zr, Mo, Ru)C with s-process enrichments of up to 200 times the solar value, indicating an AGB origin for these graphite grains. SiC subgrains were found within six different high-density graphite sections (Croat et al. 2010). Of those SiC-containing graphite grains measured for Si isotopes, two of three show extreme $^{29,30}$Si enrichments that could only originate in massive stars. In a few rare cases, kamacite, iron carbide, and metallic (Os)RuFe phases were also found (Croat et al. 2005). Additionally, subgrains have been found in SN graphite grains; all eleven low-density SN graphite grains studied

by Croat et al. (2003) contain refractory carbides, with a single graphite often containing hundreds of internal TiC subgrains. Many of these TiC subgrains (30–230 nm) have epitaxially grown kamacite and taenite grains (8–76 nm in diameter), providing clear evidence of Fe condensation in SN ejecta. Independent kamacite subgrains are also present, but are far less abundant.

Iron-nickel subgrains, which are detected as significant increases in the Fe signal in isotopic depth profiles, have been independently observed in isotopic measurements of SiC X and Z grains in the NanoSIMS (Marhas et al. 2008; Hynes et al. 2009). Most of the grains have highly anomalous Fe and Ni isotopic compositions and at least half of the X grains (and several of the Z grains) contain subgrains, which are the apparent carriers of the Fe anomalies. These subgrains show a wide range of Ni/Fe ratios, in agreement with the TEM observations in this study. However, the bulk Ni/Fe ratios of approximately 5.5 that were measured in the isotopic studies are not only much higher than the solar ratio of 0.059, but they are also much higher than those observed in this study.

While a wide array of subgrain types have been observed in presolar grains, to the best of our knowledge, this is the first reported observation of silicides. They are, however, not unexpected. Lodders (2006) predicted the formation of silicides in the C/He, Si/S, and Fe/Ni zones (named for their most abundant elements by mass) of Type II SNe as part of her calculations to explain the observations by Croat et al. (2003) of graphite containing internal TiC with attached Fe-Ni grains (suggesting a condensation sequence of TiC—metal—graphite). Several problems existed in explaining these observations. First, the calculated condensation sequence for mixtures of the He/C, O/C, and He/N zones is TiC—graphite—SiC—silicides. Also, except in the Fe/Ni zone, Si is as abundant as Fe, leading to the condensation of silicides (previously unobserved) over the observed Fe-Ni metal. Deep in the outflowing Fe/Ni zone, however, the Si abundance is so low that titanides [i.e., $(Fe,Ni)_nTi_m$] could form in place of silicides and would then need to be transported to outer zones where a thermochemically favorable reaction would convert the titanides to TiC and Fe-Ni metal grains.

Although the existence of silicides is theoretically predicted and they are expected to readily form in SNe, the question of how they are incorporated into SiC remains. Three possible scenarios exist for the formation of subgrains in an astrophysical environment: independent formation of the subgrains prior to SiC and subsequent capture via collisions and sticking, similar to TiC subgrains observed in graphite (Croat et al. 2003); heterogeneous nucleation and growth of the subgrains onto the surface of SiC, similar to the growth of kamacite grains onto TiC (Croat et al. 2003); and the formation of subgrains after SiC formation via a solid-state reaction, such as the exsolution of the silicides from solid solution at the SiC grain boundaries, similar to the formation of TiC subgrains in SiC mainstream grains (Bernatowicz et al. 1992).

Crystallographic, morphological, and chemical properties of the subgrains can help limit the possible scenarios for silicide formation. Diffraction patterns from at least two subgrains in KJG-N2-129-1 indicate a likely epitaxial relationship with the surrounding SiC. These subgrains are aligned within approximately 1–5° of the SiC plane. Other diffraction patterns from the subgrains and the surrounding SiC are inconclusive. The likelihood of a subgrain forming independently, then sticking to a SiC crystal at a random orientation that happened to be crystallographically aligned with the SiC is unlikely, and it is even more improbable that this would occur twice in a single SiC grain, effectively eliminating this scenario as a possibility for subgrain formation. Crystallographic alignment could, however, be expected for both heterogeneous nucleation and exsolution.

Examination of TEM BF images of the subgrains show that the subgrains are located at SiC crystal domain boundaries, rather than in the interior of a SiC crystal. Several of the subgrains (such as sg 4, see Fig. 9d) even have concave boundaries with the surrounding SiC domains, a clear sign of secondary formation. This morphology is not consistent with subgrains that formed independently of the SiC and were later incorporated, nor does it resemble subgrains that nucleated onto the surface of another grain, such as the kamacite subgrains on TiC grains, which are found in SN graphite grains (Croat et al. 2003).

Both the crystallographic alignment and the morphology of the subgrains suggest an exsolution process, although the considerable compositional variation among the multiple subgrains in grain KJG-N2-129-1, which are only hundreds of nanometers apart, could be explained by the formation of silicides prior to SiC. However, the compositional variation can also be explained if the grains exsolved from solid solution. Crystallographic data indicate that there is not a single equilibrium silicide phase that can form over the observed compositional range. This suggests that at a SiC grain boundary, there may not be an equilibrium phase that exists for the Ni/Fe ratio present there. The subgrain would form, for example, as an Fe-rich silicide that contains as much Ni as the phase allows, while the excess Ni is pushed out of the grain, leading to the later formation of extremely Ni-rich silicides. The

compositional data for the subgrains all fall into ranges of either high (Ni/Fe ≥ 1.6) or low (Ni/Fe ≤ 0.41) Ni/Fe ratios, but no subgrains have been observed with Ni/Fe ratios in between these values, supporting the idea that the formation of equilibrium phases may only be possible at either high or low Ni/Fe ratios.

The morphological characteristics of the subgrains, their observed compositional range, and the epitaxial alignment of the subgrains with the surrounding SiC all point towards the silicides co-condensing in solid solution with SiC and then exsolving at lower temperatures as the most likely formation mechanism for the subgrains. This scenario also agrees with the predicted formation sequence in the He/C zone of a SN in which SiC condenses before silicides (Lodders 2006). However, additional theoretical calculations, such as those recently carried out by Fedkin et al. (2009), coupled with additional observations of subgrains in SiC X grains, particularly those X grains containing multiple subgrains, are still needed to gain a more complete understanding of grain formation in SN outflows.

## SUMMARY AND CONCLUSIONS

Our TEM observations have revealed several unique characteristics of SiC X grains. The crystal domains in X grains are significantly smaller than those of SiC mainstream grains, indicating conditions of supersaturation and rapid formation in the SN environment, which is consistent with previous conclusions from both astronomical observations and isotopic measurements. Despite the fact that X grains form in the ejecta of Type II SNe, they exhibit the same polytypes as mainstream grains, which form around AGB stars. Although temperatures and pressures, which are thought to play a large role in polytype formation, are possibly quite different in AGB and SN outflows at the time of grain formation, this difference appears to have little or no effect on polytype formation in presolar SiC. This suggests either that polytype is not particularly sensitive to the range of temperatures and pressures in which SiC can condense in astrophysical environments or that other factors, such as the Si/C ratio, which may not be that different in regions of SiC formation in AGB and SN outflows, may play a more dominant role in polytype formation. Additional experimental and theoretical work is needed to determine the reason that no differences in the polytypes present in mainstream and X grains have yet been observed.

We have also observed the first subgrains in SiC X grains. These subgrains have an epitaxial relationship with the surrounding SiC crystal domains, as well as a large range of Ni/Fe ratios, even between subgrains less than a hundred nanometers apart, suggesting that they were likely present in the SiC in solid solution and later exsolved at the SiC crystal domain boundaries as discrete phases dependent upon their Ni/Fe ratios. The crystallographic data from the subgrains are inconsistent with any previously observed presolar phase. Based on their crystallographic structure, we conclude that these subgrains are silicides. Silicides are, in fact, predicted stable SN condensates, although more work needs to be done to explain their formation and incorporation into SiC. Additional subgrains from a larger suite of SiC X grains would also help in identifying specific silicide phases and providing additional compositional and morphological information. Finally, although the number of SiC X grains that have been microanalyzed has been significantly increased, the study of many additional grains is needed to provide better statistics, possibly reveal rare SiC polytypes or subgrain types that were not observed in the limited number of grains studied thus far, and generally provide a more comprehensive understanding of the formation of SiC X grains.

*Acknowledgments*—We would like to thank Roy Lewis of the University of Chicago for providing the Murchison KJG sample. We also thank Rhonda Stroud, Jan Leitner, and Ian Lyon for their helpful comments and reviews.

*Editorial Handling*—Dr. Ian Lyon

## REFERENCES

Amari S., Hoppe P., Zinner E., and Lewis R. S. 1992. Interstellar SiC with unusual isotopic compositions: Grains from a supernova? *The Astrophysical Journal* 394:L43–L46.

Amari S., Lewis R. S., and Anders E. 1994. Interstellar grains in meteorites: I. Isolation of SiC, graphite, and diamond; size distributions of SiC and graphite. *Geochimica et Cosmochimica Acta* 58:459–470.

Amari S., Hoppe P., Zinner E., and Lewis R. S. 1995. Trace-element concentrations in single circumstellar silicon carbide grains from the Murchison meteorite. *Meteoritics* 30:679–693.

Amari S., Zinner E., and Lewis R. S. 2000. Isotopic compositions of different presolar silicon carbide size fractions from the Murchison meteorite. *Meteoritics & Planetary Science* 35:997–1014.

Anikin M. and Madar R. 1997. Temperature gradient controlled SiC crystal growth. *Materials Science & Engineering B (Solid-State Materials for Advanced Technology)* B46:278–286.

Bender H., De Veirman A., Van Landuyt J., and Amelinckx S. 1986. HREM investigation of twinning in very high dose phosphorus ion-implanted silicon. *Applied Physics A (Solids and Surfaces)* A39:83–90.

Bernatowicz T. J., Amari S., and Lewis R. S. 1992. TEM studies of a circumstellar rock. Proceedings, 23rd Lunar and Planetary Science Conference. pp. 91–92.

Bernatowicz T. J., Cowsik R., Gibbons P. C., Lodders K., Fegley B. Jr., Amari S., and Lewis R. S. 1996. Constraints on stellar grain formation from presolar graphite in the Murchison meteorite. *The Astrophysical Journal* 472: 760–782.

Bernatowicz T. J., Akande O. W., Croat T. K., and Cowsik R. 2005. Constraints on grain formation around carbon stars from laboratory studies of presolar graphite. *The Astrophysical Journal* 631:988–1000.

Bernatowicz T. J., Croat T. K., and Daulton T. L. 2006. Origin and evolution of carbonaceous presolar grains in stellar environments. In *Meteorites and the early solar system II*, edited by Lauretta D. S. and McSween Jr. H. Y. Tucson, AZ: The University of Arizona Press. pp. 109–126.

Croat T. K., Bernatowicz T. J., Amari S., Messenger S., and Stadermann F. J. 2003. Structural, chemical, and isotopic microanalytical investigations of graphite from supernovae. *Geochimica et Cosmochimica Acta* 67:4705–4725.

Croat T. K., Stadermann F. J., and Bernatowicz T. J. 2005. Presolar graphite from AGB stars: Microstructure and s-process enrichment. *The Astrophysical Journal* 631: 976–987.

Croat T. K., Stadermann F. J., and Bernatowicz T. J. 2010. Unusual 29,30 Si-rich SiCs of massive star origin found within graphites from the Murchison meteorite. *The Astrophysical Journal* 139:2159–2169.

Daulton T. L., Bernatowicz T. J., Lewis R. S., Messenger S., Stadermann F. J., and Amari S. 2003. Polytype distribution of circumstellar silicon carbide: Microstructural characterization by transmission electron microscopy. *Geochimica et Cosmochimica Acta* 67: 4743–4767.

Daulton T. L., Stadermann F. J., Bernatowicz T. J., Amari S., and Lewis R. S. 2006. First systematic TEM-NanoSIMS coordinated study of crystal structure and isotopic composition of presolar silicon carbide (abstract). *Meteoritics & Planetary Science* 41:A42.

Daulton T. L., Stadermann F. J., Bernatowicz T. J., Amari S., and Lewis R. S. 2009. Coordinated TEM/NanoSIMS microanalysis of structurally or isotopically rare presolar silicon carbide (abstract). *Meteoritics & Planetary Science* 72:5381.

Ebel D. S. and Grossman L. 2000. Condensation in dust-enriched systems. *Geochimica et Cosmochimica Acta* 64:339–366.

Fedkin A. V., Meyer B. S., Grossman L., and Desch S. J. 2009. Condensation in supernova ejecta at high spatial resolution (abstract #1699). 40th Lunar and Planetary Science Conference. CD-ROM.

Fisher G. R. and Barnes P. 1990. Towards a unified view of polytypism in silicon carbide. *Philosophical Magazine B (Physics of Condensed Matter, Electronic, Optical and Magnetic Properties)* 61:217–236.

Fissel A. 2000. Thermodynamical consideration of the epitaxial growth of SiC polytypes. Proceedings, International Conference on Silicon Carbide and Related Materials. pp. 209–212.

Heine V., Cheng C., and Needs R. J. 1991. The preference of silicon carbide for growth in the metastable cubic form. *Journal of the American Ceramic Society* 74:2630–2633.

Hoppe P. and Besmehn A. 2002. Evidence for extinct vanadium-49 in presolar silicon carbide grains from supernovae. *The Astrophysical Journal* 576:L69–L72.

Hoppe P. and Ott U. 1997. Mainstream silicon carbide grains from meteorites. In *Astrophysical implications of the laboratory study of presolar materials*, edited by Bernatowicz T. J. and Zinner E. New York: American Institute of Physics. pp. 27–58.

Hoppe P., Amari S., Zinner E., Ireland T., and Lewis R. S. 1994. Carbon, nitrogen, magnesium, silicon, and titanium isotopic compositions of single interstellar silicon carbide grains from the Murchison carbonaceous chondrite. *The Astrophysical Journal* 430:870–890.

Hoppe P., Strebel R., Eberhardt P., Amari S., and Lewis R. S. 1996. Small SiC grains and a nitride grain of circumstellar origin from the Murchison meteorite: Implications for stellar evolution and nucleosynthesis. *Geochimica et Cosmochimica Acta* 60:883–907.

Hynes K. M. and Gyngard F. 2009. The Presolar Grain Database: http://presolar.wustl.edu/~pgd (abstract #1198). 40th Lunar and Planetary Science Conference. CD-ROM.

Hynes K. M., Croat T. K., Amari S., Mertz A. F., and Bernatowicz T. J. 2006. A transmission electron microscope study of internal subgrains in SiC-X grains (abstract). *Meteoritics & Planetary Science* 41:A83.

Hynes K. M., Gyngard F., Zinner E., and Nittler L. R. 2009. Iron and nickel isotopic compositions of silicon carbide Z grains (abstract #5168). *Meteoritics & Planetary Science* 44:A96.

Kern R. S., Tanaka S., Rowland L. B., and Davis R. F. 1998. Reaction kinetics of silicon carbide deposition by gas-source molecular-beam epitaxy. *Journal of Crystal Growth* 183:581–593.

Krishna P. and Marshall R. C. 1971. Direct transformation from the 2H to the 6H structure in single-crystal silicon carbide. *Journal of Crystal Growth* 11:147–150.

Krishna P., Marshall R. C., and Ryan C. E. 1971. The discovery of 2H-3C solid state transformation in silicon carbide single crystals. *Journal of Crystal Growth* 8:129–131.

Lattimer J. M., Schramm D. N., and Grossman L. 1978. Condensation in supernova ejecta and isotopic anomalies in meteorites. *The Astrophysical Journal* 219:230–249.

Lin Y., Amari S., and Pravdivtseva O. 2002. Presolar grains from the Qingzhen (EH3) meteorite. *The Astrophysical Journal* 575:257–263.

Lodders K. 2003. Solar system abundances and condensation temperatures of the elements. *The Astrophysical Journal* 591:1220–1247.

Lodders K. 2006. They came from the deep in the supernova: The origin of TiC and metal subgrains in presolar graphite grains. *The Astrophysical Journal* 647:L37–L40.

Lodders K. and Fegley B. Jr. 1995. The origin of circumstellar silicon carbide grains found in meteorites. *Meteoritics* 30:661–678.

Marhas K. K., Amari S., Gyngard F., Zinner E., and Gallino R. 2008. Iron and nickel isotopic ratios in presolar SiC grains. *The Astrophysical Journal* 689:622–645.

Meyer B. S. and Zinner E. 2006. Nucleosynthesis. In *Meteorites and the early solar system II*, edited by Lauretta D. S. and McSween Jr. H. Y. Tucson, AZ: The University of Arizona Press. pp. 69–108.

Meyer B. S., Weaver T. A., and Woosley S. E. 1995. Isotope source table for a 25 $M_{\odot}$ supernova. *Meteoritics* 30: 325–334.

Miura H., Kato M., and Mori T. 1990. Determination of boundary energies of Cu from the shape of boundary $SiO_2$ particles. *Colloque de Physique* 1:263–268.

Nittler L. R., Hoppe P., Alexander C. M. O'D., Amari S., Eberhardt P., Gao X., Lewis R. S., Strebel R., Walker R. M., and Zinner E. 1995. Silicon nitride from supernovae. *The Astrophysical Journal* 453:L25–L28.

Nittler L. R., Amari S., Zinner E., Woosley S. E., and Lewis R. S. 1996. Extinct $^{44}$Ti in presolar graphite and SiC: Proof of a supernova origin. *The Astrophysical Journal* 462:L31–L34.

Patrick L., Hamilton D. R., and Choyke W. J. 1966. Growth, luminescence, selection rules and lattice sums of SiC with wurtzite structure. *Physical Review* 143:528–536.

Sharp C. M. and Wasserburg G. J. 1995. Molecular equilibria and condensation temperatures in carbon-rich gases. *Geochimica et Cosmochimica Acta* 59:1633–1652.

Speck A. K., Hofmeister A. M., and Barlow M. J. 1999. The SiC problem: Astronomical and meteoritic evidence. *The Astrophysical Journal* 513:L87–L90.

Stan M. A., Patton M. O., Warner J. D., Yang J. W., and Pirouz P. 1994. Growth of 2H-SiC on 6H-SiC by pulsed laser ablation. *Applied Physics Letters* 64:2667–2669.

Stroud R. M. and Bernatowicz T. J. 2005. Surface and internal structure of pristine presolar silicon carbide (abstract #2010). 36th Lunar and Planetary Science Conference. CD-ROM.

Stroud R. M. and Nittler L. R. 2004. A search for solar-system processing signatures in presolar grains (abstract #9091). Proceedings, Workshop on Chondrites and the Protoplanetary Disk.

Stroud R. M., O'Grady M., Nittler L. R., and Alexander C. M. O'D. 2002. Transmission electron microscopy of an in situ presolar silicon carbide grain (abstract #1785). 33rd Lunar and Planetary Science Conference. CD-ROM.

Stroud R. M., Nittler L. R., and Hoppe P. 2004. Microstructures and isotopic compositions of two SiC X grains (abstract). *Meteoritics & Planetary Science* 39:A101.

Wooden D. H. 1997. Observational evidence for mixing and dust condensation in core-collapse supernovae. In *Astrophysical implications of the laboratory study of presolar materials*, edited by Bernatowicz T. J. and Zinner E. New York: American Institute of Physics. pp. 317–374.

Yoo W. S. and Matsunami H. 1991. Polytype-controlled single-crystal growth of silicon carbide using $3C \rightarrow 6H$ solid-state phase-transformation. *Journal of Applied Physics* 70:7124–7131.

Zangvil A. and Ruh R. 1988. Phase relationships in the silicon carbide-aluminum nitride system. *Journal of the American Ceramic Society* 71:884–890.

Zhaoqing L. and Jun N. 2005. Layered growth modelling of epitaxial growth processes for SiC polytypes. *Journal of Physics: Condensed Matter* 17:5355–5366.

Zinner E., Amari S., Guinness R., Jennings C., Mertz A. F., Nguyen A. N., Gallino R., Hoppe P., Lugaro M., Nittler L. R., and Lewis R. S. 2007. NanoSIMS isotopic analysis of small presolar grains: Search for $Si_3N_4$ grains from AGB stars, and Al and Ti isotopic compositions of rare presolar SiC grains. *Geochimica et Cosmochimica Acta* 71:4786–4813.